The response of precipitation characteristics to global warming from climate projections

Filippo Giorgi, Francesca Raffaele, Erika Coppola

1 Earth System Physics Section, The Abdus Salam International Centre for Theoretical Physics, I-34151 Trieste, Italy

Corresponding author: Filippo Giorgi, Earth System Physics Section, The Abdus Salam International Centre for Theoretical Physics, Trieste, I-34151, Italy. Email: giorgi@ictp.it; phone: +39 0402240425.

Submitted to: Earth System Dynamics

Abstract

We revisit the issue of the response of the precipitation characteristics to global warming based on analyses of global and regional climate model projections for the 21st century. The prevailing response we identify can be summarized as follows: increase in the intensity of precipitation events and extremes, with the occurrence of events of "unprecedented" magnitude, i.e. magnitude not found in present day climate; decrease in the number of light precipitation events and in wet spell lengths; increase in the number of dry days and dry spell lengths. This response, which is mostly consistent across the models we analyzed, is tied to the difference between precipitation intensity responding to increases in local humidity conditions and circulations, especially for heavy and extreme events, and mean precipitation responding to slower increases in global evaporation. These changes in hydroclimatic characteristics have multiple and important impacts on the Earth's hydrologic cycle and on a variety of sectors, and as examples we investigate effects on the potential stress due to increases in dry and wet extremes, changes in precipitation interannual variability and changes in potential predictability of precipitation events. We also stress how the understanding of the hydroclimatic response to global warming can shed important insights into the fundamental behavior of precipitation processes, most noticeably tropical convection.

Keywords: Precipitation, climate change, hydrologic cycle, extremes

1. Introduction

One of the greatest concerns regarding the effects of climate change on human societies and natural ecosystems is the response of the Earth's hydrologic cycle to global warming. In fact, by affecting the surface energy budget, greenhouse gas (GHG) induced warming, along with related feedback processes (e.g. the water vapor, ice albedo and cloud

feedbacks), can profoundly affect the Earth's water cycle (e.g. Trenberth et al. 2003; Held and Soden 2006; Trenberth 2011; IPCC 2012).

The main engine for the Earth's hydrologic cycle is the radiation from the Sun, which heats the surface and causes evaporation from the oceans and land. Total surface evaporation has been estimated at 486 10^3 km^3/year of water, of which 413 10^3 km^3/year, or ~85%, is from the oceans and the rest from land areas (Trenberth et al. 2007). Once in the atmosphere, water vapor is transported by the winds until it eventually condenses and forms clouds and precipitation. The typical atmospheric lifetime of water vapor is of several days, and therefore at climate time scales there is essentially an equilibrium between global surface evaporation and precipitation. Total mean precipitation as been estimated at 373 10^3 km^3/year of water over oceans and 113 10^3 km^3/year over land (adding up to the same global value as evaporation, Trenberth et al. 2007). Water precipitating over land can then either re-evaporate or flow into the oceans through surface runoff or sub-surface flow.

Given this picture of the hydrologic cycle, however, it is important to stress that, although evaporation and precipitation globally balance out, their underlying processes are very different. Evaporation is a continuous and slow process (globally about ~2.8 mm/day, Trenberth et al. 2007), while precipitation is a highly intermittent, fast and localized phenomenon, with precipitation events drawing moisture only from an area of about 3-5 times the size of the event itself (Trenberth et al. 2003). In addition, on average, only about 25% of days are rainy days, but since it does not rain throughout the entire day, the actual fraction of time it rains has been estimated at 5-10% (Trenberth et al. 2003). In other words, most of the time it does not actually rain.

This has important implications for the assessment of hydroclimatic responses to global warming, because it may not be very meanigful, and certainly not sufficient, to analyze

mean precipitation fields, but it is necessary to also investigate higher order statistics. For example, the same mean of, say, 1 mm/day could derive from 10 consecutive 1 mm/day events, a single 10 mm/day event with 9 dry days, or two 5 mm/day events separated by a dry period. Each of these cases would have a very different impact on societal sectors or ecosystem dynamics.

This consideration also implies that the impact of global warming on the Earth's hydroclimate might actually manifest itself not only as a change in mean precipitation but, perhaps more markedly, as variations in the characteristics and regimes of precipitation events. This notion has been increasingly recognized since the pioneering works of Trenberth (1999) and Trenberth et al. (2003), with many studies looking in particular at changes in the frequency and intensity of extreme precipitation events (e.g. Easterling et al. 2000; Christensen and Christensen 2003; Tebaldi et al. 2006; Allan and Soden 2008; Giorgi et al. 2011; IPCC 2012; Sillmann et al. 2013; Giorgi et al. 2014a,b; Pendergrass and Hartmann 2014; Sedlacek and Knutti 2014; Pfahl et al. 2017; Thackeray et al. 2018).

In this paper, which presents a synthesis of the Alexander von Humboldt medal lecture given by the first author (FG) at the European Geosciences Union (EGU) General Assembly of 2018, we revisit some of the concepts related to the issue of the impacts of global warming on the characteristics of the Earth's hydroclimate, stressing however that it is not our purpose to provide a review of the extensive literature on this topic. Rather, we want to illustrate some of the points made above through relevant examples obtained from new and past analyses of global and regional climate model projections carried out by the authors.

More specifically, we will draw from global climate model (GCM) projections carried out as part of the CMIP5 program (Taylor et al. 2012) and regional climate model (RCM) projections from the COordinated Regional climate Downscaling EXperiment (CORDEX,

86 Giorgi et al. 2009; Jones et al. 2011, Gutowski et al. 2016), which downscale CMIP5 GCM
87 data. In this regard, we focus on the high end RCP8.5 scenario, in which the ensemble mean
88 global temperature increase by 2100 is about 4^{o}C (+/- 1^{o}C) compared to late 20th century
89 temperatures (IPCC 2013), stressing that results for lower GHG scenarios are qualitatively
90 similar to those found here but of smaller magnitude (not shown for brevity).

91 In the next sections we first summarize the changes in mean precipitation fields in our
92 ensemble of model projections, and then explore the response of different precipitation
93 characteristics, trying specifically to identify robust responses. After having identified the
94 dominant hydroclimatic responses, we discuss examples of their impact on different quantities
95 of relevance for socio-economic impacts, and specifically the potential stress associated with
96 changes in dry and wet extreme events, precipitation interannual variability and predictability
97 of precipitation events.

98 **2. The hydroclimatic response to global warming**

99 Throughout this paper we mostly base our analysis on the 10 CMIP5 GCMs used by
100 Giorgi et al. (2014b) for easier comparison with, and reference to, this previous work. These
101 10 models were chosen because they were the only ones among the full CMIP5 dataset for
102 which daily data were available at the time the analysis of Giorgi et al (2014b) was carried
103 out. This sub-ensemble includes some of the most commonly used models, and an analysis of
104 mean and seasonal data by Giorgi et al. (2014b) showed that it behaves quite similarly to the
105 full CMIP5 ensemble. In addition, as will be seen later, a high level of consistency is found in
106 the behavior of these models also concerning daily statistics, and therefore we feel that this
107 10-GCM ensemble is at least qualitatively representative of the full CMIP5 set.

108 ***2.1 Mean precipitation changes***

In general, as a result of the warming of the oceans and land, global surface evaporation increases with increasing GHG forcing. This increase mostly lies in the range of 1-2 % per degree of surface global warming (%/DGW; Trenberth et al. 2007). As a consequence, global mean precipitation also tends to increase roughly by the same amount. This has been found in most GCM projections, as illustrated in the examples of Figure 1.

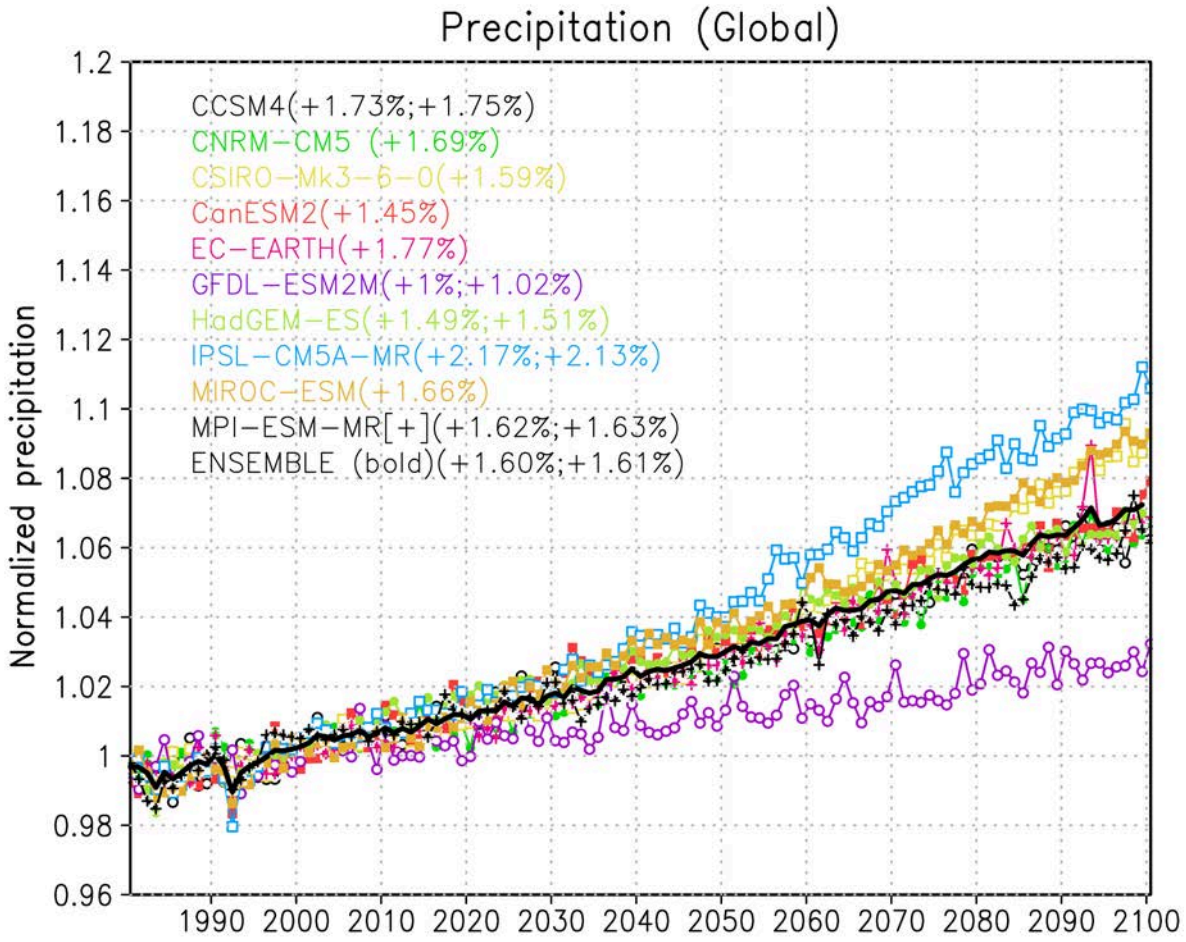

Figure 1. Normalized mean global precipitation from 1981 to 2100 in the 10 CMIP5 GCMs simulation for the RCP8.5 scenario used by Giorgi et al. (2014b), along with their ensemble average. The first number in parentheses shows the corresponding mean global precipitation change per degree of global warming, while the second shows (for a subset of models with available data) the same quantity for global surface evaporation. The annual precipitation is normalized by the mean precipitation during the reference period 1981-2010, therefore a value of, e.g., 1.1 indicates an increase of 10%.

Although precipitation increases globally, at the regional level we can find relatively complex patterns of change, with areas of increased and areas of decreased precipitation. These patterns are closely related to changes in global circulation features, global energy and

momentum budgets, local forcings (e.g. topography, land use) and energy and water fluxes affecting convective activity (e.g. Thackeray et al. 2018). The basic geographical structure of precipitation change patterns has been quite resilient throughout different generations of GCM projections, at least in an ensemble averaged sense. These precipitation change patterns are shown in Figure 2 as obtained from the CMIP5 ensemble, but they are similar in the CMIP3 and earlier GCM ensembles.

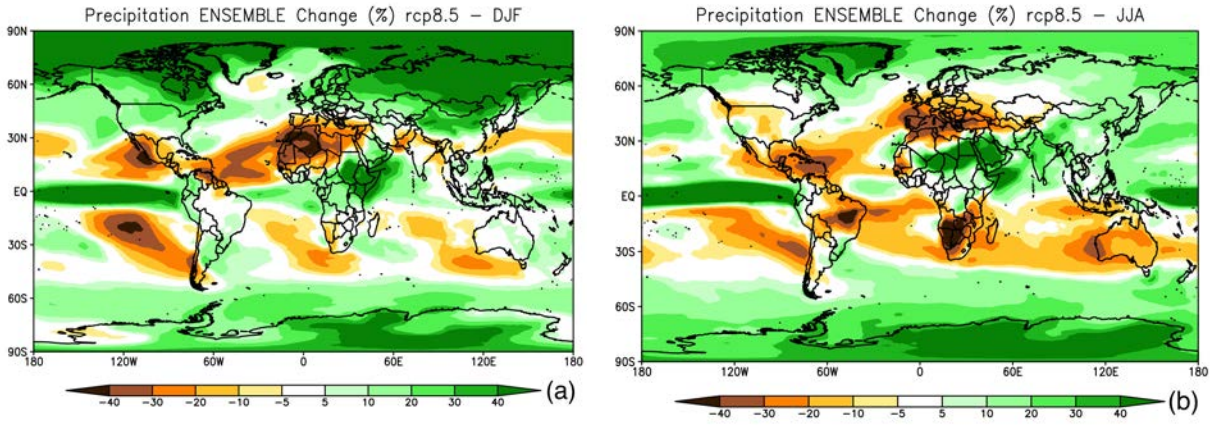

Figure 2. Ensemble mean change in precipitation (RCP8.5, 2071-2100 minus 1981-2010) for December-January-February (panel a) and June-July-August (panel b) in the CMIP5 ensemble of models.

The increase in precipitation at mid to high latitudes has been attributed to a poleward shift of the storm tracks associated with maximum warming in the tropical troposphere (due to enhanced convection), which in turn produces a poleward shift of the maximum horizontal temperature gradient and jet stream location (e.g. IPCC 2013). This process is essentially equivalent to a poleward expansion of the Hadley Cell, which also causes drier conditions in sub-tropical areas, including the Mediterranean and Central America/Southwestern U.S. regions. The Intertropical Convergence Zone (ITCZ) shows narrowing and greater precipitation intensity, especially in the core of the Pacific ITCZ, associated with increased organized deep convective activity towards the ITCZ center and decreased activity along its edges (Byrne et al. 2018). Finally, over monsoon regions, a general increase of precipitation has been attributed to a greater water-holding capacity of the atmosphere counterbalancing a

144 decrease in monsoon circulation strength (IPCC 2013), however more detailed analyses of
145 how global constraints on energy and momentum budgets affect regional scale circulations
146 are needed for a better understanding of the monsoon response to global warming (Biasutti et
147 al. 2018).

148 As already mentioned, these broad scale change patterns have been confirmed by
149 different generations of GCM projections, and thus appear to be robust model-derived signals.
150 On the other hand, high resolution RCM experiments have shown that local forcings
151 associated with complex topography and coastlines can substantially modulate these large
152 scale signals, often to the point of being of opposite sign. For example, the precipitation
153 shadowing effect of major mountain systems tends to concentrate precipitation increases
154 towards the upwind side of the mountains, and to reduce the increases or even generate
155 decreases of precipitation in the lee side (e.g. Giorgi et al. 1994; Gao et al. 2006). Similarly, in
156 the summer, the precipitation change signal can be strongly affected by high elevation
157 warming and wetting which enhance local convective activity. For example, Giorgi et al.
158 (2016) found enhanced precipitation over the Alpine high peaks in high resolution EURO-
159 CORDEX (Jacob et al. 2014) and MED-CORDEX (Ruti et al. 2016) projections, whereas the
160 driving coarse resolution global models produced a decrease in precipitation. In addition to
161 these local effects, it has been found that the simulation of some modes of variability, such as
162 blocking events, is also sensitive to model resolution (e.g. Anstey et al. 2013, Schiemann et al.
163 2017). As a result of all these processes it is thus possible that the large scale precipitation
164 change patterns of Fig. 2 might be significantly modified as we move to substantially higher
165 resolution models.

166 On the other hand, a key question concerning the precipitation response to global
167 warming is: "How will precipitation change patterns affect different socioeconomic sectors?".
168 This question depends more on the modifications of the characteristics of precipitation than

169 the mean precipitation itself. For example, changes in precipitation interannual variability
170 may have strong impacts on crop planning. As another example, if an increase in precipitation
171 is due to an increase of extreme damaging events, this will have negative rather than positive
172 impacts. Alternatively, if the increase is due to very light events that do not replenish the soil
173 of moisture, this will not constitute an added water resource. Conversely, a reduction of
174 precipitation mostly associated with a reduction of extremes will result in positive rather than
175 negative impacts. It is thus critical to assess how the characteristics of precipitation will
176 respond to global warming, which is the focus of the next sections.

177 ***2.2 Daily precipitation intensity Probability Density Functions (PDFs)***

178 Daily precipitation is one of the variables most often used in impact assessment
179 studies, therefore an effective way to investigate the response of precipitation characterstics to
180 global warming is to assess changes in daily precipitation intensity PDFs. As an illustrative
181 example of PDF changes, Figures 3 and 4 show normalized precipitation intensity PDFs for 4
182 time slices, 1981-2010 (reference period representative of present day conditions), 2011-2040,
183 2041-2070 and 2071-2100 in the MPI-ESM-MR RCP8.5 projection of the CMIP5 ensemble.
184 The farther the time slice is in the future, the greater the warming (up to a maximum of about
185 4 °C in 2071-2100). The variable shown, which we refer to as PDF, is the frequency of
186 occurrence of precipitation events within a certain interval (bin) of intensity normalized by the
187 total number of days, including non-precipitating days.

188 Note that in the MPI-ESM-MR model the response of mean global precipitation to
189 global warming is in line with the model ensemble average (Figure 1), while the response of
190 daily statistics is among the strongest (e.g. see Giorgi et al. 2014b and Table 1), but
191 qualitatively consistent with most other models (see below). Therefore this model is well

illustrative of the simulated precipitation response to global warming in the sub-set of CMIP5 GCMs analyzed.

Also, as in our previous work (Giorgi et al. 2014b), throughout this paper a rainy day is considered has having a precipitation amount of at least 1 mm/day, so that drizzle days are removed. In this regard, the choice of a precipitation threshold to define a rainy day makes the calculation of precipitation frequency and intensity dependent on the resolution of the data (e.g. Chen and Dai 2018). Attention should be paied to this issue when analyzing precipitation statistics and here, as well as in previous work, we conduct direct cross model or data-model intercomparisons only after having interpolated the data onto common grids.

Finally, given the logarithmic scale of the frequency of occurrence, in order to better illustrate changes in frequencies, Figures 3 and 4 report the ratio of the frequency of occurrence for a given bin in a future time slice divided by the same quantity in the reference period. Averaged data are shown for land areas in the tropics (30^{o}S-30^{o}N, Figure 3), and extra-tropical midlatitudes (30-60^{o} N and S, Figure 4), noting that qualitatively similar results were found for ocean areas.

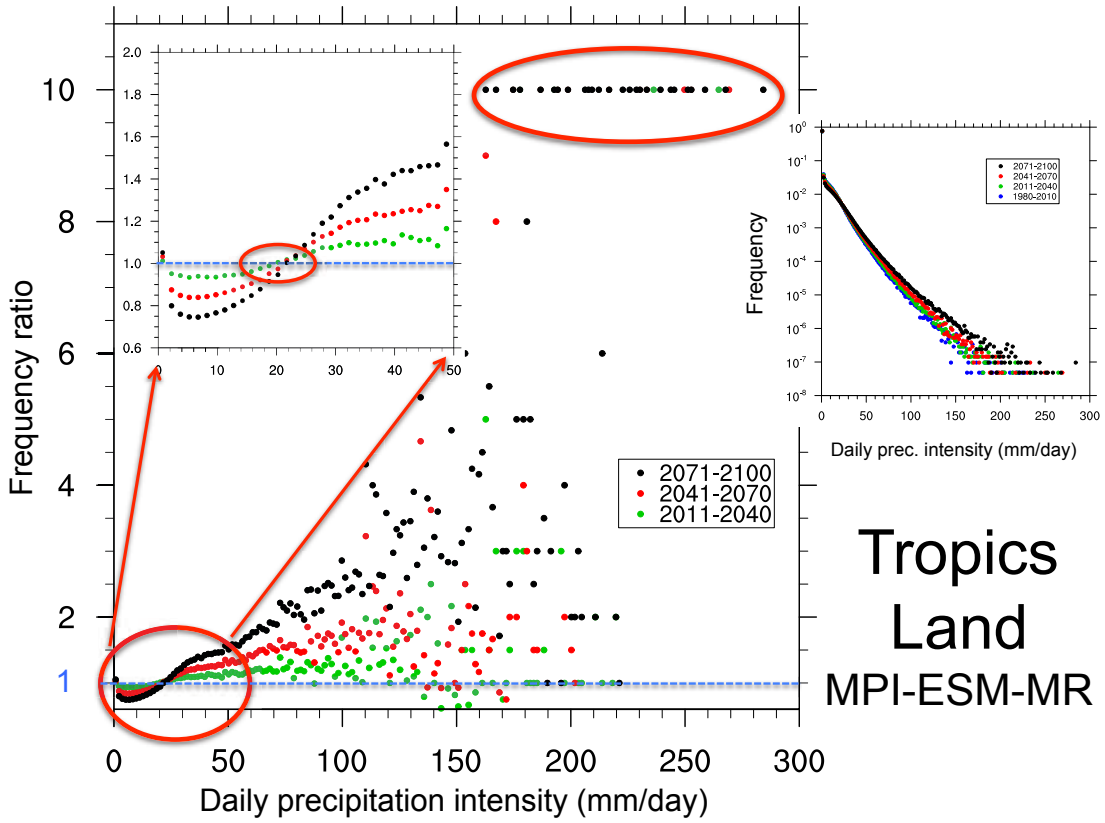

209

210

211 **Figure 3.** Small right panel: Probability density function (PDF) defined as the normalized frequency of
212 occurrence of daily precipitation events of intensity within a certain bin interval over land regions in the tropics
213 (30°S - 30°N) for the reference period 1981-2010 and three future time slices (2011-2040, 2041-2070, 2071-
214 2100) in the MPI-ESM-MR model. The frequency is normalized by the total number of days (including dry days,
215 i.e. days with precipitation lower than 1 mm/day). Large central panel: Ratio of future to reference normalized
216 frequency of daily precipitation intensity for the three future time slices. The small inset panel shows a zoom on
217 the part of the curves highlighted by the corresponding red oval. Ratio values of 10 (hilighted in a red oval) are
218 used when events occur in the future time slice which are not present in the reference period for a given intensity
219 bin.

220

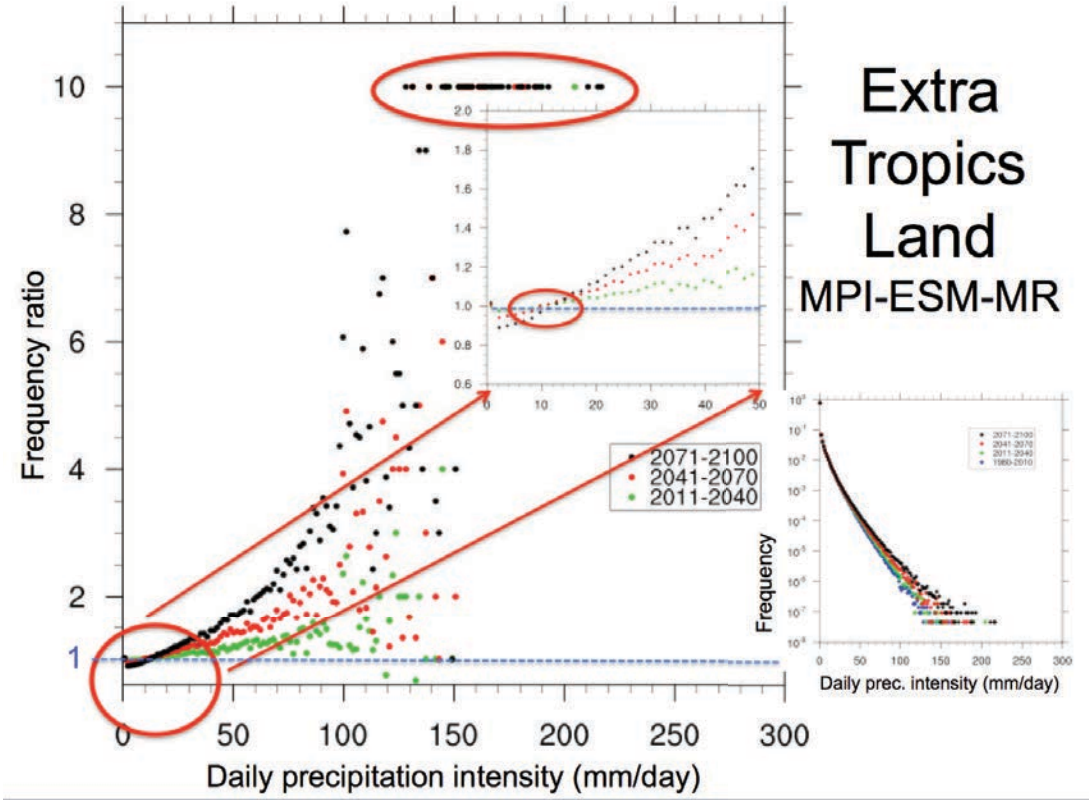

Figure 4. Same as Figure 3 but for extra-tropical land areas.

The PDFs exhibit a log-linear relationship between intensities and frequencies, with a sharp drop in frequency as the intensity increases. The ratios of future vs. present day frequencies consistently show the following features:

i) An increase in the number of dry days, as seen from the ratios > 1 in the first bin (precipitation less than 1 mm/day), i.e. a decrease in the frequency of wet events. Note that, even if these ratios are only slightly greater than 1, because the frequencies of dry days are much higher than those of wet days, the actual absolute increase in the number of dry days is relatively high.

ii) A decrease (ratio < 1) in the frequency of light to medium precipitation events up to a certain intensity threshold. In the models we analyzed, when taken over large areas, this threshold lies around the 95th percentile of the full distribution, and is higher for tropical than

235 extratropical land regions because of the higher amounts of precipitation in tropical
236 convection systems. Interestingly, while the threshold depends on latitude, it is approximately
237 invariant for all future time slices, i.e. it appears to be relatively independent of the level of
238 warming. The decrease in light precipitation events has been at least partially attributed to an
239 increase in thermal stability induced by the GHG forcing (Chou et al. 2012).

240 iii) An increase (ratio > 1) in the frequency of events for intensities higher than the
241 threshold mentioned above. The relative increase in frequency grows with the intensity of the
242 events, and it is thus maximum for the highest intensity events, an indication of a non linear
243 response of the precipitation intensity to warmer conditions. Note that, because of the
244 logarithmic frequency scale, the absolute increase in the number of high intensity events is
245 relatively low.

246 iv) The occurrence in the future time slices of events with intensity well beyond the
247 maximum found in the reference period. These are illustrated by the prescribed value of 10
248 when events occurred for a given bin in the future time slice, but not in the reference one. One
249 could thus interpret these as occurrences of "unprecedented" events.

250 v) All the features i)-iv) tend to amplify as the time slice is further into the future, i.e.
251 as the level of warming increases, and are generally more pronounced over tropical than
252 extratropical areas (and over land than ocean regions, which we did not show for brevity).

253 Although the results in Figures 3 and 4 are obtained from one model, they are
254 qualitatively consistent with those we found for other CMIP5 GCMs. As example, results
255 analogous to those of Figures 3 and 4, but for the HadGEM and EC-Earth GCMs, are reported
256 in Supplementary figures S1 and S2. We also carried out the same type of analysis for a high
257 resolution RCM projection (12 km grid spacing, RCP8.5 scenario) conducted with the
258 RegCM4 model (Giorgi et al. 2012) over the Mediterranean domain defined for the MED-
259 CORDEX program (Ruti et al. 2016). Figures 5 and 6 show PDFs and PDF ratios for three
260 30-year future time slices calculated over land areas throughout the Mediterranean domain

and over a sub-area covering the Alpine region. They show features similar to those found for the GCMs, with the signal over the Alpine region being more pronounced than for the entire Mediterranean area. As further examples, Supplementary Figures S3 and S4 report similar plots computed over the entire European land territory for EURO-CORDEX simulations with the REMO and RACMO RCMs, which show features qualitatively in line with those of Figures 5 and 6. In addition, our results are also consitent with previous analyses of RCM projections (e.g. Gutowski et al. 2007; Boberg et al. 2009; Jacob et al 2014; Giorgi et al. 2014a), suggesting that the projected changes in precipitation intensity PDFs summarized in the points i)-iv) above are generally robust across a wide range of models and model resolutions.

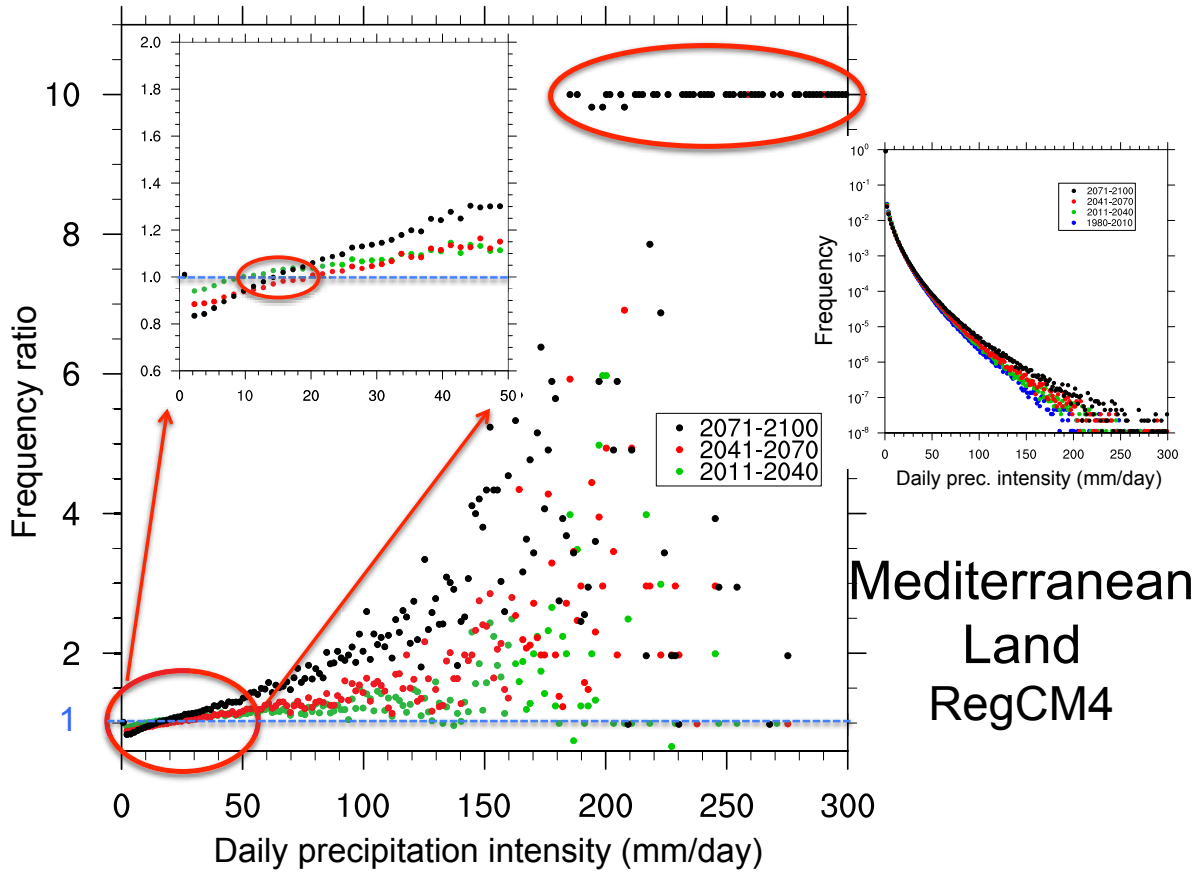

Figure 5. Same as Figure 3 but for Mediterranean land areas in a MED-CORDEX experiment with the RegCM4 RCM driven by global fields from the HadGEM GCM.

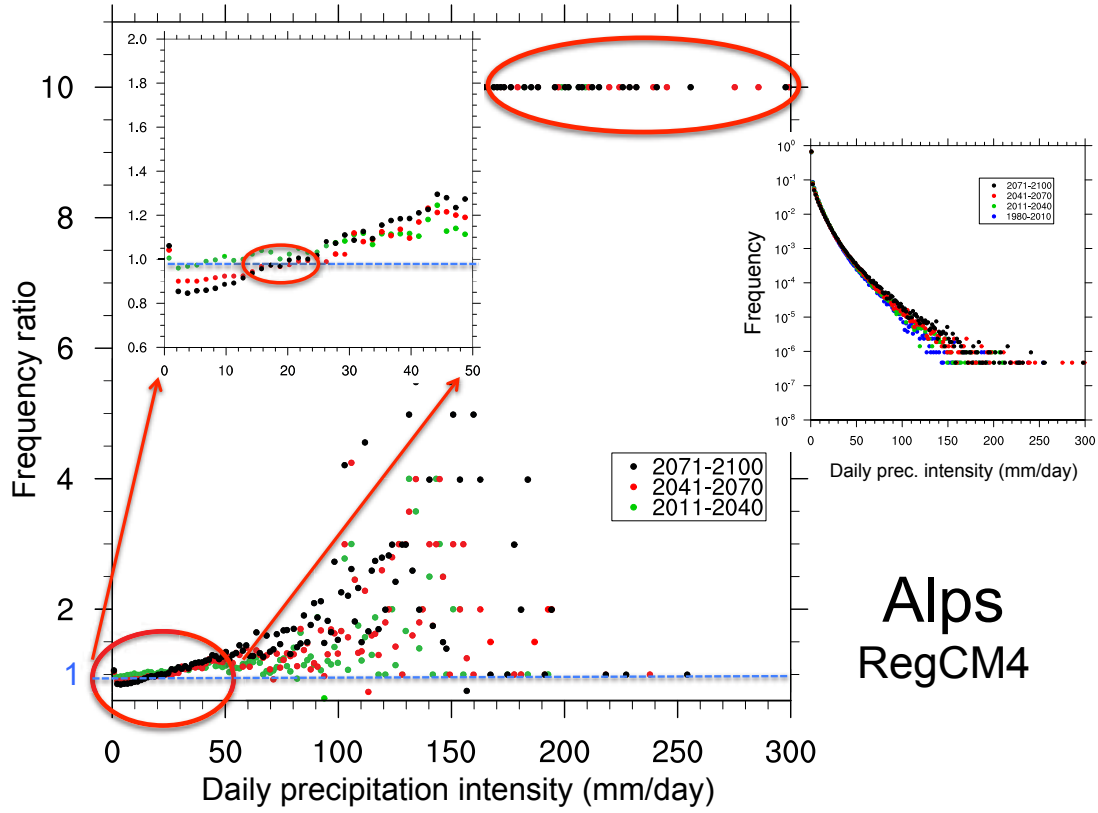

Figure 6. Same as Figure 5 but for the Alpine region.

2.3 Hydroclimatic indices

The changes in precipitation intensity PDFs found in the previous section should be reflected in, and measured by, changes of hydroclimatic indices representative of given precipitation regimes. In two previous studies (Giorgi et al. 2011, 2014b), we assessed the changes of a series of interconnected hydroclimatic indices in an ensemble of 10 CMIP5 projections. The indices analyzed include:

SDII: Mean precipitation intensity (including only wet events)

DSL: Mean dry spell length, i.e. mean length of consecutive dry days

WSL: Mean wet spell length, i.e. mean length of consecutive wet days

R95: Fraction of total precipitation above the 95th percentile of the daily precipitation intensity distribution during the reference period 1981-2010.

PA: Precipitation area, i.e. the total area covered by wet events at any given day

HY-INT, i.e. the hydroclimatic intensity index introduced by Giorgi et al. (2011) consisting of the product of normalized SDII and DSL.

Note that the PA and HY-INT indices were specifically introduced by Giorgi et al. (2011, 2014b). The PA is the spatial counterpart of the mean frequency of precipitation days, while the HY-INT was introduced under the assumption that the changes in SDII and DSL are interconnected responses to global warming (Giorgi et al. 2011).

Giorgi et al. (2011, 2014b) examined changes in these indices for ensembles of CMIP3 and CMIP5 GCM projections, as well as a number of RCM projections, in future time slices with respect to the 1976-2005 reference period. Their results, which were consistently found for most models analyzed, indicated a prevalent increase in SDII, R95, HY-INT and DSL and a decrease in PA and WSL. Similar results where then found by Giorgi et al. (2014a) in an analysis of multiple RegCM4-based projections over 5 CORDEX domains. In other words, under warmer climate conditions, precipitation events are expected to be more intense and extreme, and temporally more concentrated and less frequent, which implies a reduction of the areas occupied by rain at any given time (although not necessarily a reduction of the size of the events). This response, which is consistent with the change in PDFs illustrated in Figures 3-6, will be hereafter referred to as the higher intensity - reduced frequency (HIRF) precipitation response.

Giorgi et al. (2011 and 2014b) also analyzed a global and several regional daily precipitation gridded observation datasets, and found that trends for the period 1976-2005 were predominantly in line with the model projected changes over most continental areas.

315 Further evidence of increases in heavy precipitation events in observational records is for
316 example reported by Fischer and Knutti (2016) and references therein, however this
317 conclusion cannot be considered entirely robust, and needs to be verified with further
318 analysis, due to the high uncertainty in precipitation observations (e.g. Herold et al. 2017).

319 An explanation for the HIRF hydroclimatic response to global warming is related to
320 the fact that, on the one hand, the mean global precipitation change roughly follows the mean
321 global evaporation increase, i.e. 1.5-2.0 %/DGW (Trenberth et al. 2007, Figure 1). On the
322 other hand, the intensity of precipitation, in particular for high and extreme precipitation
323 events, is more tied to the increase in the water holding capacity of the atmosphere, which is
324 in turn regulated by the Clausius-Clapeyron (Cl-Cl) response of about 7%/DGW, although the
325 precipitation response is modulated by regional and local circulations, along with energy and
326 water fluxes, which might lead to super- or sub- Cl-Cl responses (e.g. Trenberth et al. 2003;
327 Pall et al. 2007; Lenderink and van Meijgaard 2008; Chou et al. 2012; Singleton and Toumi
328 2013; Pendergrass and Hartmann 2014; Ivancic and Shaw 2016; Fischer and Knutti 2016;
329 Pfahl et al. 2017). Therefore the increase in precipitation intensity can be expected to be
330 generally larger than the increase in mean precipitation, which implies a decrease in
331 precipitation frequency.

332 To illustrate this point, Table 1 reports the globally averaged changes (2071-2100
333 minus the reference period 1976-2005, as in Giorgi et al. 2014b; RCP8.5 scenario) in mean
334 precipitation, precipitation intensity and frequency, and the 95th, 99th and 99.9th percentiles
335 of daily precipitation for the 10 GCMs of Giorgi et al. (2014b), along with their ensemble
336 average. The values of Table 1 were calculated as follows: we first computed the change in
337 %/DGW at each model grid point and then averaged these values over global land+ocean as
338 well as global land-only areas. This was done in order to avoid the possiblity that areas with
339 large precipitation amounts may dominate the average. On the other hand, grid-point

340 normalization artificially amplifies the contribution of regions with small precipitation
341 amounts, such as polar and desert areas. For this reason, as in Giorgi et al. (2014b), we did not
342 include in the averaging areas north of 60^{o}N and south of 60 ^{o}S (polar regions) along with
343 areas with mean annual precipitation lower than 0.5 mm/day (which effectively identifies
344 desert regions). In addition, we did not consider precipitation associated with days with
345 amounts of less than 1 mm/day in order to be consistent with our definition of rainy day
346 (which disregards drizzle events).

347

Global Box						
Models	N. Wet Days %/ DGW	Precipitation change (due to wet days)%/ DGW	SDII change(%)/ DGW	95p change(%)/ DGW	99p change(%)/ DGW	99.9p change(%)/ DGW
HadGEM-ES	-0.7	1.3	1.8	1.7	2.9	3.9
MPI-ESM-MR	-2.4	1.0	3.5	1.9	3.7	5.3
GFDL-ESM2M	-1.4	0.05	1.2	0.3	2.1	10.4
IPSL-CM5A-MR	-1.0	1.6	2.6	2.0	4.5	7.9
CCSM4	-1.1	0.7	1.8	1.1	2.8	5.5
CanESM2	-0.4	1.6	1.7	1.5	2.5	4.4
EC-EARTH	-0.9	1.3	2.1	1.9	3.7	5.9
MIROC-ESM	0.2	1.4	0.9	1.1	1.2	1.6
CSIRO-Mk3-6-0	-0.6	0.8	1.9	2.3	2.4	3.4
CNRM-CM5	-0.1	1.4	1.5	1.5	2.9	5.8
ENSEMBLE	**-0.8**	**1.1**	**1.9**	**1.5**	**2.9**	**5.4**

Global LAND Box						
Models	N. Wet Days %/ DGW	Precipitation change (due to wet days)%/ DGW	SDII change(%)/ DGW	95p change(%)/ DGW	99p change(%)/ DGW	99.9p change(%)/ DGW
HadGEM-ES	-1.4	0.7	2.1	1.2	2.8	4.5
MPI-ESM-MR	-3.3	0.1	4.0	0.8	3.7	5.4
GFDL-ESM2M	-1.8	1.1	3.1	1.2	4.5	12.4
IPSL-CM5A-MR	-1.8	0.7	2.5	1.2	3.8	7.2
CCSM4	-0.6	1.3	1.9	1.3	2.8	5.4
CanESM2	-0.6	1.2	1.7	1.3	3.4	5.0
EC-EARTH	-0.8	1.4	2.3	2.0	3.8	6.0
MIROC-ESM	0.2	1.8	1.4	1.1	1.7	2.1
CSIRO-Mk3-6-0	-1.8	-0.2	1.5	0.2	1.1	2.4
CNRM-CM5	0.4	2.5	2.0	2.0	3.2	6.0
ENSEMBLE	**-1.2**	**1.1**	**2.3**	**1.2**	**3.1**	**5.6**

Table 1. Change in different daily precipitation indicators between 2071-2100 and 1976-2005 for the 10 CMIP5 GCMs of Giorgi et al. (2014b) expressed in % per degree of surface global warming over global (upper box) and global-land (lower box) areas, where global means the area between 60°S and 60°N. SDII is the precipitaiton intensity, 95p, 99p and 99.9p are the 95th, 99th and 99.9th percentiles, respectively, and the precipitation change only include wet days, i.e. days with precipitation greater than 1 mm/day.

Also in these calculations, the increase in global mean precipitation is in the range of 1-2 %/DGW except for the GFDL experiment, which shows a very small increase (indicating that in this model most of the precipitation increase occurs in the polar regions). In all cases except for MIROC the increase in global SDII is greater than the increase in mean

358 precipitation, resulting in a decrease of the number of rainy days. The changes in the 95th,
359 99th and 99.9th percentile are maximum for the most extreme percentiles, showing that the
360 main contribution to the HIRF response is due to the highest intensity events, i.e. above the
361 99th and 99.9th percentiles, whose response becomes increasingly closer to the Cl-Cl one
362 (and even super Cl-Cl for the GFDL model). In fact, the increase in 95th percentile for the
363 ensemble model average is lower than the increase in SDII, and this is because in some
364 models the threshold intensity in Figures 3-6, where the sign of the change turns from
365 negative to positive, lies beyond the 95th percentile. When only land areas between 60^{o}S and
366 60^{o}N are taken into account (bottom panel in Table 1), the changes are generally in line with
367 the global ones, except for the CNRM model. Over land areas we also find changes in the
368 highest percentiles of magnitude mostly greater than over the globe (and thus over oceans).

369 We can thus conclude that the shift to a regime of more intense but less frequent
370 events in warmer conditions is due to the fact that precipitation intensity, especially for
371 intense events (beyond the 95th percentile), responds at the local level primarily to the Cl-Cl-
372 driven increase of water vapor amounts modulated by local circulations and fluxes, while
373 mean precipitation responds to a slower evaporation process, driving a decrease in
374 precipitation frequency. Noticeably, the MIROC experiment does not appear to follow this
375 response, i.e. in this model the increase in mean precipitation appears to be driven by an
376 increase in the number of light precipitation events.

377 While the data of Table 1 provide a diagnostic explanation of the HIRF response, it
378 has also been suggested by very high resolution convection-permitting simulations that ocean
379 temperatures might affect the self-organization and aggregation of convective systems (e.g.
380 Mueller and Held 2012; Becker et al. 2017), which would also affect the precipitation
381 response to warming. Therefore, the study of the HIRF response might lead to a greater

382 understanding of the fundamental behavior of the precipitation phenomenon, and in particular
383 of tropical convection processes.

384 **3. Some consequences of the hydroclimatic response to global warming**

385 What are the consequences of the HIRF response to global warming? Obviously there
386 can be many of them, but here we want to provide a few illustrative examples of relevance for
387 impact applications.

388 ***3.1 Potential stress associated with wet and dry extreme events.***

389 The HIRF response suggests that global warming might induce an increase in the risk
390 of damaging extreme wet and dry events, the former being associated with the increase in
391 precipitation intensity, and latter with the occurrence of longer sequences of dry days over
392 areas of increasing size. In order to quantify this risk, in a recent paper (Giorgi et al. 2018,
393 hereafter referred to as GCR18) we introduced a new index called the Cumulative
394 Hydroclimatic Stress Index, or CHS. In GCR18, the CHS was calculated for two types of
395 extreme events, the 99.9th percentile of the daily precipitation distribution (or R99.9) and the
396 occurrence of at least three consecutive months experiencing a precipitation deficit of
397 magnitude greater than 25% of the precipitation climatology for that months (or D25). Both of
398 these metrics thus refer to extremely wet and dry events which can be expected to produce
399 significant damage (see GCR18).

400 Taking as an example the R99.9, the CHS essentially cumulates the excess
401 precipitation above the 99.9th percentile threshold calculated for a given reference period (e.g.
402 1981-2010). Hence, the assumption is that the potential stress associated with these extremes
403 is proportional to the excess precipitation above the 99.9 percentile of the distribution. GCR18
404 calculated this quantity for a future climate projection, and then normalized it by the
405 corresponding value cumulated over the reference period. This normalization expresses the

potential stress due to the increase in wet extremes in Equivalent Reference Stress Years (ERSY), where an ERSY is the mean stress per year due to the extremes during the reference period (in our case 1981-2010). If, for example, a damage value can be associated to such events, the ERSY can be interpreted as the mean yearly damage caused by extremes in present climate conditions. GCR18 then carried out similar calculations for the cumulative potential stress due to dry events by cumulating the deficit rain defined by the D25 metric. In addition, similarly to Diffenbaugh Et al. (2007) and Sedlacek and Knutti (2014), they included exposure information within the definition of the CHS index by multiplying the excess or deficit precipitation by future population amounts (as obtained from Shared Socioeconomic Pathways, or SSP, Rihai et al. 2016) normalized by present day population values. The details of these calculations can be found in GCR18.

The main results of GCR18 are summarized in Figures 7 and 8, which present maps of the potential cumulative stress due to both dry and wet events added by climate change during the period 2010-2100 and expressed in added ERSY (i.e. after removing the value of 90 that would be obtained if no climate change occurred). The figures show the total ensemble-averaged added cumulative stress for the RCP8.5 scenario without (Figure 7) and with (Figure 8) inclusion of population weighting (where the SSP5 population scenario from Rihai et al. 2016 was used). The values in the figures were computed by first calculating the stress contribution in ERSY of wet and dry extremes separately and then adding them, so that there is no cancellation of stress if, say, a wet extreme is followed by a dry extreme.

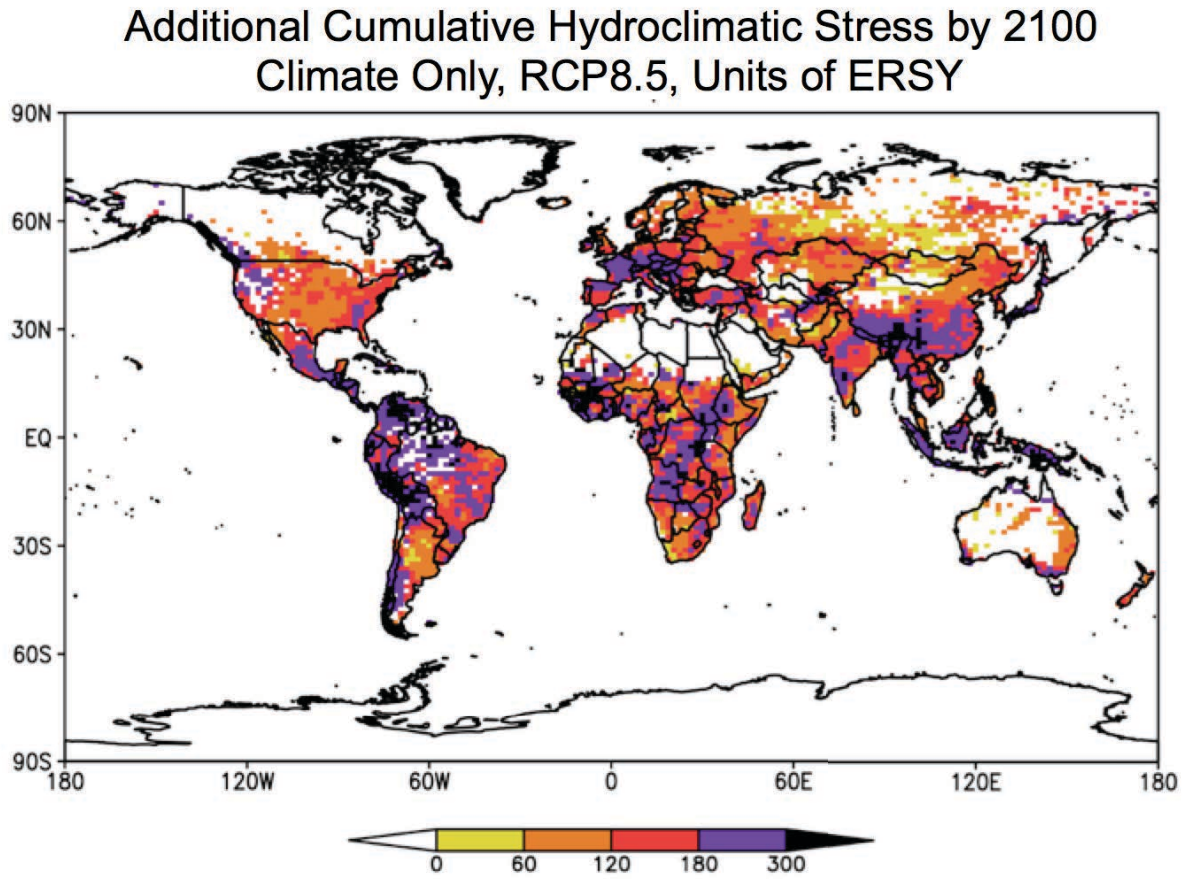

426 **Figure 7.** Total number of additional stress years due to increases in wet (R99.9) and dry (D25) events
427 for the period 2011 - 2100 including only climate variables for the RCP8.5 scenario (see text for more detail).
428 Units are Equivalent Reference Stress Years (ERSY) and the value does not include ERSY obtained if climate
429 did not change (i.e. for the period 2100 - 2011 a value of 90).

430

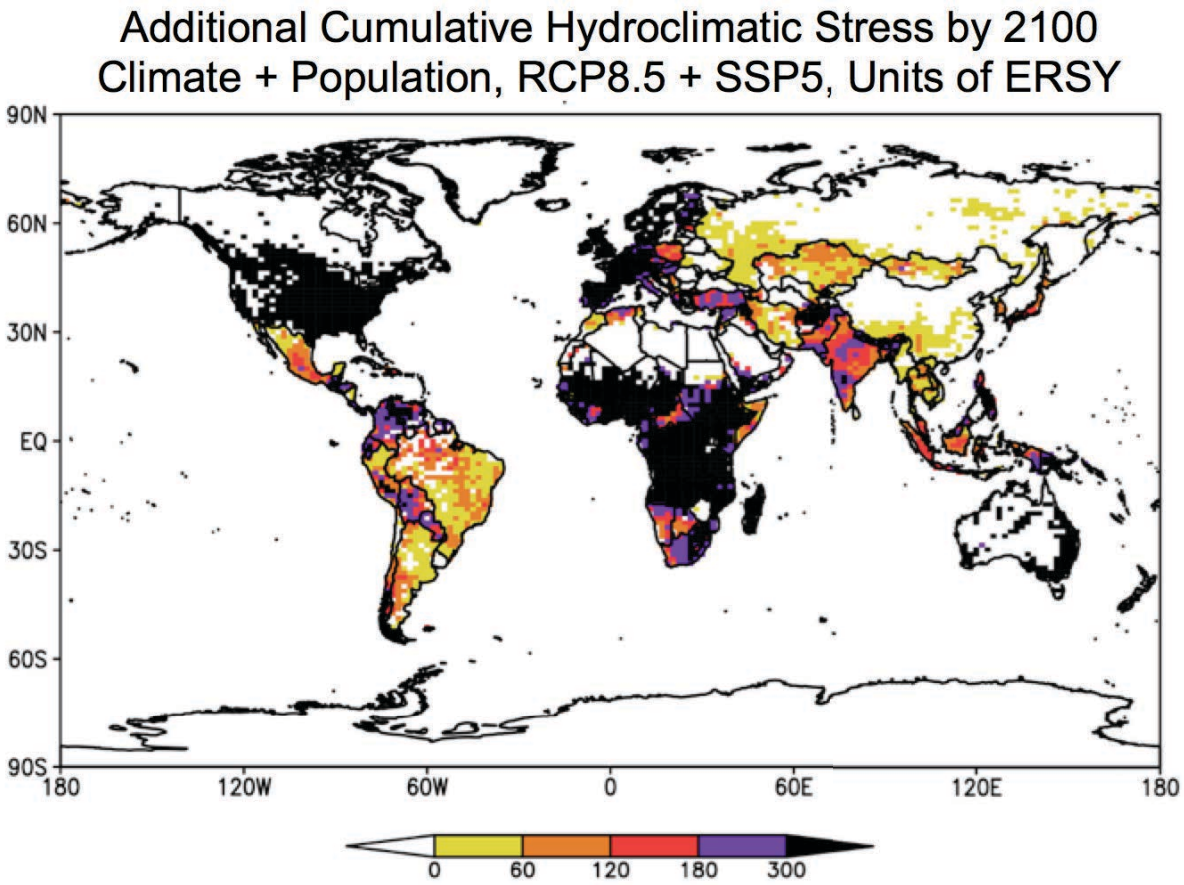

Figure 8. Same as Figure 8, but with the inclusion of the SSP5 population scenario (see text for more detail).

Figure 7 shows that, when only climate is accounted for, dry and wet extremes add more than 180 ERSY (and in some cases more than 300 ERSY) over extended areas of Central and South America, Europe, Western and south/central Africa, Southern and Southeastern Asia. In other words, the combined potential stress due to dry and wet extremes more than triples due to climate change by the end of the century. In this regard, GCR18 found that, when globally averaged over land regions and over all the models considered, both wet and dry extremes increased in the RCP8.5 scenario, the former adding ~120 ERSY, while the latter adding ~30 ERSY.

When population scenarios are also accounted for (Figure 8) the patterns of added cumulative stress are considerably modified. In this case, the total number of added ERSY exceeds 300 over the entire continental U.S. and Canada, most of Africa, Australia and areas of South and Souteast Asia, which are projected to experience substantial population increases in the SSP5 scenario. Conversely, we find a reduced increase in stress over East and Southeast Asia, where population is actually projected to decrease by the end of the 21st century (see GCR18). This result thus points to the importance of incorporating socio-economic information in the assessment of the stress associated with climate change-driven extreme events.

Notwithstanding the limitations and approximations of the approach of GCR18, amply discussed in that paper, the results of Figures 7 and 8 clearly indicate that the increase of wet and dry extremes associated with global warming can constitute a serious threat to the socio-economic development of various regions across all continents. GCR18 also show that the cumulative stress due to increases in extremes is drastically reduced under the RCP2.6 scenario, pointing to the importance of mitigation measures to reduce the level of global warming.

3.2 Impact on interannual variability.

The interannual variability of precipitation is a key factor affecting many aspects of agriculture and water resources and it is strongly affected by global modes of variability, such as the El Nino Southern Oscillation (ENSO) in the tropics and the North Atlantic Oscillation (NAO) in mid-latitudes. In this regard, the latest generation of GCM projections does not provide definitive indications concerning changes in the frequency or intensity of such modes (e.g. IPCC 2013), although some works suggest the presence of robust changes in projected

466 spatial patterns of ENSO-driven precipitation and temperature variability (e.g. Power et al.
467 2013).

468 Daily and seasonal precipitation statistics are not necessarily tied, since the same
469 seasonal mean can be obtained via different sequences of daily precipitation events. In
470 addition, the intensity distribution of daily and seasonal precipitation amounts can be quite
471 different, the latter being often close to normal distributions (e.g. Giorgi and Coppola 2009).
472 On the other hand, the occurrence of longer dry spells, intensified by higher temperatures and
473 lower soil moisture amounts, might be expected to amplify dry seasons, while the increase in
474 the intensity of sequences of wet events might lead to amplified wet seasons. As a result, it
475 can be expected that the HIRF regime response might lead to an increase in precipitation
476 interannual variability.

477 To verify this hypothesis, we calculated for the GCM ensemble of Giorgi et al.
478 (2014b) the change in precipitation interannual variability between future and present day 30-
479 year time slices using as metric the coefficient of variation (CV). The CV is defined as the (in
480 our case interannual) standard deviation normalized by the mean, and has been often used as a
481 measure of precipitation variability because it removes the strong dependence of precipitation
482 variability on the mean itself (Raisanen 2002; Giorgi and Bi 2005).

483

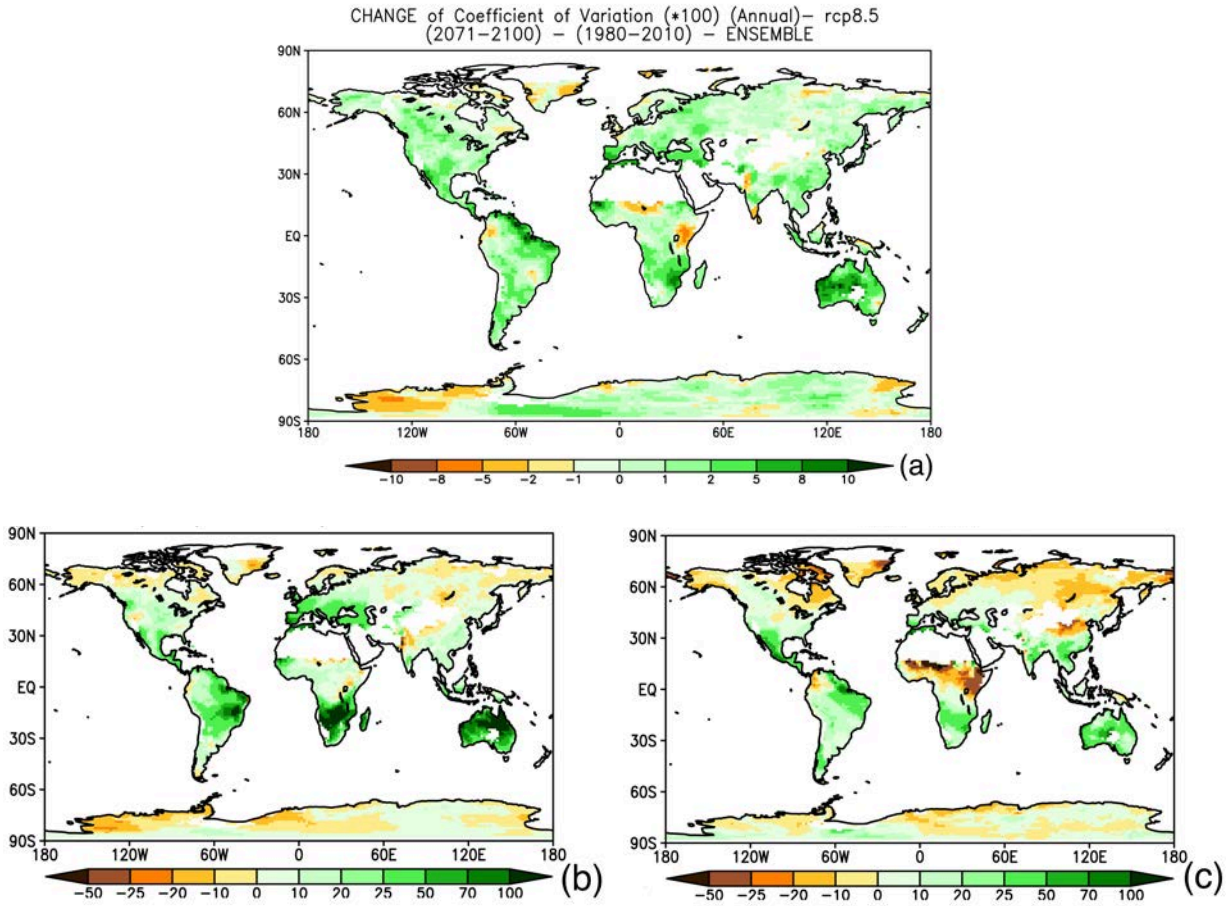

Figure 9. Change in precipitation interannual coefficient of variation (2071-2100 vs. 1981-2010) for a) mean annual precipitation; b) April-September precipitation; c) October-March precipitation.

Figure 9 shows the ensemble average change in precipitation CV between the 2071-2100 and 1981-2010 time slices for mean annual precipitation as well as precipitation averaged over the two 6-month periods Apr-Sept and Oct-Mar. It can be seen that, when considering annual averages, the interannual variability increases over the majority of land areas, with exceptions over small regions scattered throughout the different continents. When considering the two different 6-month seasons, in Apr-Sept (northern hemisphere summer, southern hemisphere winter) variability increases largely dominate, except over areas of the northern hemisphere high latitudes and some areas around major mountain systems. In Oct-

496 Mar, the areas of decreased variability are more extended over northern Eurasia, northern
497 North America and, interestingly, some equatorial African regions, although still the increases
498 are somewhat more widespread.

499 Although Figure 9 does not show a signal of ubiquitous sign across all land areas, it
500 clearly points to a prevalent increase in interannual variability associated with global
501 warming, at least as measured by the CV. It is important to notice that this increase occurs in
502 areas of both increased and decreased mean precipitation (see Figure 2), so that it is not
503 strongly related to the use of the CV as a metric. Finally, this result is broadly consistent with
504 analyses of previous generation model projections (Raisanen 2002; Giorgi and Bi 2005;
505 Pendegrass et al. 2017), which adds robustness to this conclusion.

506 ***3.2 Impact on precipitation predictability.***

507 A third issue we want to address concerns the possible effects of regime shifts on the
508 predictability of precipitation, an issue which has obvious implications for a number of socio-
509 economic activities (e.g. agriculture, hazards, tourism etc.). Indeed, precipitation is one of the
510 most difficult meteorological variables to forecast, since it depends on both large scale and
511 complex local scale processes (e.g. topographic forcing). While the chaotic nature of the
512 atmosphere provides a theoretical limit to weather prediction of ~10-15 days (e.g. Warner
513 2010), the predictability range of different types of precipitation events depends crucially on
514 the temporal scale of the dynamics related to the event itself. For example, the predictability
515 range of synoptic systems is of the order of days, while that of long-lasting weather regimes,
516 such as blockings, can be of weeks. It is thus clear that changes in precipitation regimes and
517 statistics can lead to changes in the potential predictability of precipitation.

518 One of the benchmark metrics that is most often used to assess the skill of a prediction
519 system is persistence (Warner 2010). Essentially, persistence for a lead time T assumes that a

given weather condition at a time t+T is the same as that at time t. In other words, when applied for example to daily precipitation, it assumes that, for a lead time of N days, if day *i* is wet (dry), day *i* + N, will also be wet (dry). The skill of a forecast system is then measured by how much the forecast improves upon persistence. Therefore, persistence can be considered as a "minimum potential predictability".

In order to assess whether global warming affects what we defined minimum potential predictability for precipitation, we calculated the percentage of successfull precipitation forecasts obtained from persistence at lead times of 1, 3 and 7 days for the 10 GCM projections (RCP8.5) used by Giorgi et al. (2014). This percentage, calculated year-by-year and then averaged over all land areas, is presented in Figure 10, noting that the persistence forecast only concerns the occurrence of precipitation and not the amount.

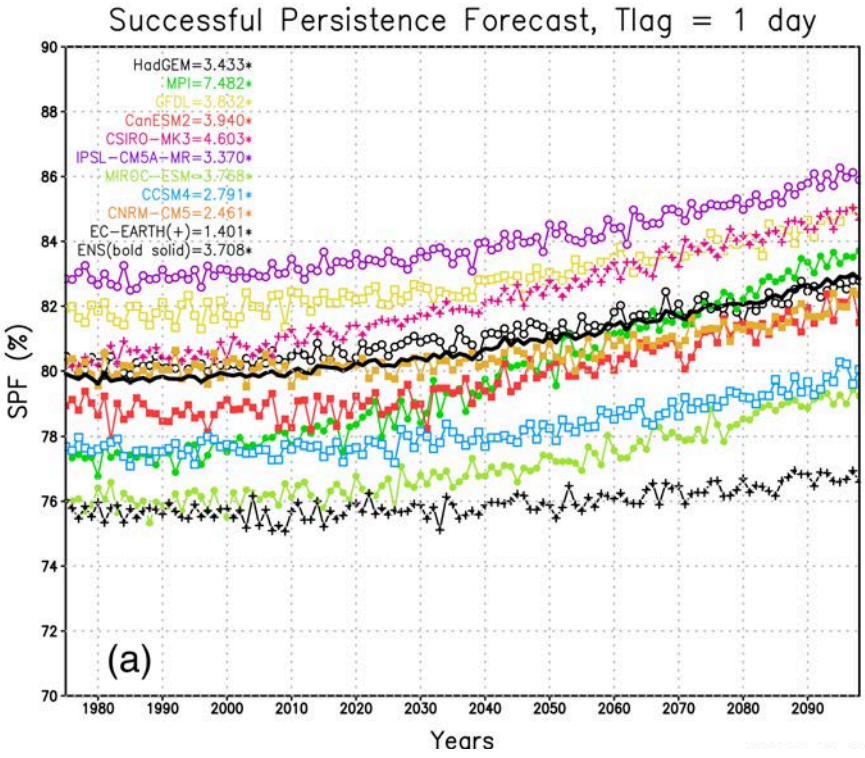

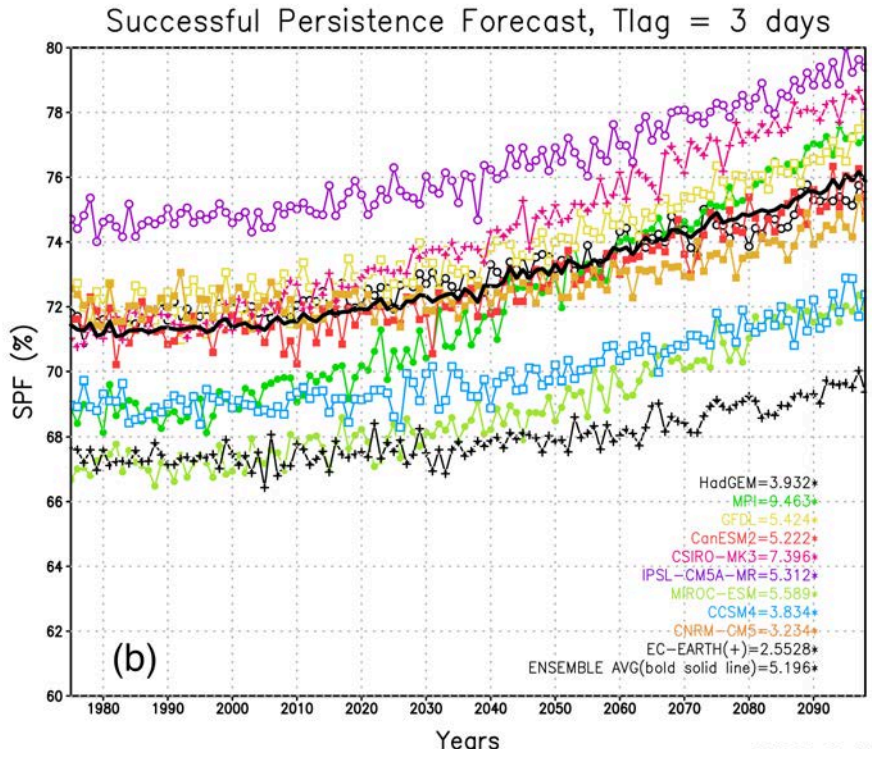

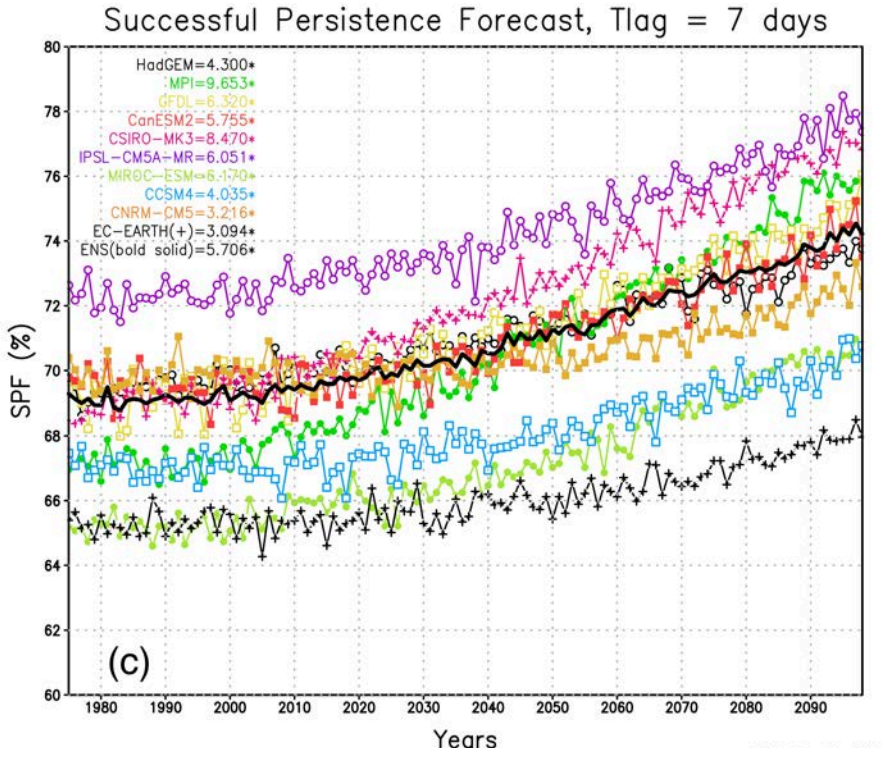

Figure 10. Fraction of successfull forecasts as a function of time using persistence for daily precipitation occurrence at time lags of a) 1 day; b) 3 days; and c) 7 days, for the GCM ensemble of Giorgi et al (2014b) (bold black line). The number in parenthesis denotes the trend in % per 100 years. Units are percentage of days in one year for which persistence provides a successful forecast (either dry or wet).

Figure 10 shows that in all model projections, and thus in the ensemble averages, the percent of successfull persistence forecasts increases with global warming for all three time lags. This can be mostly attributed to the increase in mean dry spell length found in section 2. For a lag time of 1 day, the successfull persistence forecast in the model ensemble increases globally from about 80% in 2010 to about 83% in 2100, i.e. with a linear trend of ~ 3.5 %/100 yrs. As can be expected, the % of successfull persistence forecasts decreases with the length of lag time, ~76% and 69% on 2010 for lag times of 3 and 7 days, respectively. However the growth rate of this percentage also increases with lag time, 5.2%/100 yrs and 5.7%/100 yrs for lag times of 3 and 7 days, respectively.

Despite the simplicity of the reasoning presented in this section, our results indicate that global warming can indeed affect (and in our specific case, increase) the potential predictability of the occurrence of dry vs. wet days. For example, persistence for the 7 day lag time has the same successfull forecast rate by the middle of the 21st century as the present day persistence for the 3 day lag time (~71%). Clearly, the issue of the effects of climate change on weather predictability is a very complex one, with many possible implications not only from the application point of view, but also for the assessment of the performance of forecast systems. It is thus important that this issue is addressed with more advanced techniques and metrics than we employed in our illustrative example.

4. Concluding remarks

In this paper we have revisited the basic responses of the characteristics of the Earth's hydroclimatology to global warming through the analysis of global and regional climate model projections for the 21st century. The projections examined suggested some robust hydroclimatic responses, in the sense of being mostly consistent across different model

563 projections and being predominant over the majority of land areas. They can be summarized
564 as follows:

565 1) A decrease (increase) in the frequency of wet (dry) days

566 2) An increase in the mean length of dry spells

567 3) An increase of the mean intensity of precipitation events

568 4) An increase in the intensity and frequency of wet extremes

569 5) A decrease in the frequency of light to medium precipitation events

570 6) A decrease in the mean length of wet events and in the mean area covered by
571 precipitation

572 7) Occurrence of wet events of magnitude beyond that found in present climate
573 conditions

574 We discussed how this response is mostly tied to the different natures of the
575 precipitation and evaporation processes, and we also presented some illustrative examples of
576 the possible consequences of these responses, including an increase in the risks associated
577 with wet and dry extremes, a predominant increase in the interannual variability of
578 precipitation and a modification of the potential predictability of precipitation events. In
579 addition, some of the results 1)-7) above are consistent with previous analyses of global and
580 regional model projections (e.g. Tebaldi et al. 2006; Gutowski et al. 2007; Giorgi et al.
581 2011,2014a,b; Sillmann et al. 2013a; Pendegrass and Hartmann 2014).

582 Clearly, model projections indicate that the characteristics of precipitation are going to
583 be substantially modified by global warming, most likely to a greater extent than mean
584 precipitation itself. Whether these changes are already evident in the observational record is

still an open debate. Giorgi et al. (2011, 2014b) found some consistency between model projections and observed trends in different precipitation indices for the period 1976 - 2005 in a global and some regional observational datasets. Some indications of observed increases in precipitation extremes over different regions of the World have also been highlighted in different IPCC reports (IPCC 2007, 2013) and, for example, in Fischer and Knutti (2016). In addition, data from the Munich reinsurance company suggest an increase in the occurrence of meteorological and climatic catastrophic events, such as flood and drought, since the mid-eighties. However, the large uncertainty and diversity in precipitation observational estimates, most often blending in situ station observations and satellite-derived information using a variety of methods, along with the paucity of data coverage in many regions of the World and the large variability of precipitation, make robust statements on observed trends relatively difficult.

A key issue concerning precipitation projections is the representation of cloud and precipitation processes in climate models. These processes are among the most difficult to simulate, because they are integrators of different physical phenomena and, especially for convective precipitation, they occur at scales that are smaller than the resolution of current GCMs and RCMs. For example, the representation of clouds and precipitation is the main contributor to a model's climate sensitivity and the simulation of precipitation statistics is quite sensitive to the use of different cumulus parameterizations (e.g. Flato et al. 2013). In fact, both global and regional climate models have systematic errors in the simulation of precipitation statistics, such as an excessive number of light precipitation events and an underestimate of the intensity of extremes (Kharin et al. 2005; Flato et al. 2013, Sillmann et al. 2013b). These systematic biases are related non only to the relatively coarse model resolution, but also to inadequacies of resolvable scale and convective precipitation parameterizations (e.g. Chen and Knutson 2008; Wehner et al. 2010; Flato et al. 2013).

610 Experiments with non-hydrostatic RCMs run at convection-permitting resolutions (1-3
611 km), in which cumulus convection schemes are not utilized and convection is explictly
612 resolved with non-hydrostatic wet dynamics, have shown that some characteristics of
613 simulated precipitation are strongly modified compared to coarser resolution models, most
614 noticeably the precipitation peak hourly intensity and diurnal cycle (e.g. Prein et al. 2015). It
615 is thus possible that some conclusions based on coarse resolution models might be modified
616 as more extensive experiments at convection permitting scales, both global and regional,
617 become available.

618 Despite these difficulties and uncertainties, and given the problems associated with
619 retrieving accurate observed estimates of mean precipitation at continental to global scales,
620 robust changes in different characteristics of precipitation (rather than the mean) may provide
621 the best opportunity to detect and attribute trends in the Earth's hydrological cycle. Moreover,
622 the investigation of the response of precipitation to warming may provide an important tool
623 towards a better understanding and modeling of key hydroclimatic processes, most noticeably
624 tropical convection. The ability of simulating given responses of precipitation characteristics
625 can also provide an important benchmark to evaluate the performance of climate models in
626 describing precipitation and cloud processes. Therefore, as more accurate observational
627 datasets become available, along with higher resolution and more comprehensive GCM and
628 RCM projections, the understanding of the response of the Earth's hydroclimate to global
629 warming, and its impacts on human societies, will continue to be one of the main research
630 challenges within the global change debate.

631 **Acknowledgements**

632 We thank the CMIP5 and MED-CORDEX modeling groups for making available the
633 simulation data used in this work, which can be found at the web site http://cmip-

pcmdi.llnl.gov/cmip5/data_portal.html and https://www.medcordex.eu/medcordex.php. A good portion of the material presented in this paper is drawn from the European Geosciences Union (EGU) 2018 Alexander von Humboldt medal lecture delivered by one of the authors (F.G.).

Competing Financial Interests

The authors declare no competing financial interests.

References

Allan, R.P., and Soden, B.J,: Atmospheric warming and the amplification of precipitation extremes, Science, 321, 1481-1484, 2008.

Anstey, J.A., Davini, P., Grey, L.J., Woollings, T.J., Butchart, N., Cagnazzo, C., Christiansen, B., Hardiman, S.C., Osprey, S.M., and Yang, S. : (2013). Multi-model analysis of northern hemisphere winter blocking: Model biases and the role of resolution, J. Geophys. Res. Atmos., 118, 3956-3971, 2013.

Becker, T., Stevens, B., and Hohenegger, C. : Imprint of the convective parameterization and sea surface temperature on large scale convective self-aggregation, J. Adv. Model Earth Syst., 9, 1488-1505, 2017.

Biasutti, M., Voigt, A., Boos, W.R., Bracconot, P., Hargreaves, J.C., Harrison, S.P., Kang, S.M., Mapes, B.E., Scheff, J., Schumacher, C., Sobel, A.H., and Xie, S.-P.: Global energetics and local physics as drivers of past, present and future monsoons, Nat. Geosci., 11, 392-400, 2018.

656 Boberg, F., Berg, P., Thejll, P., Gutowski, W.J., and Christensen, J.H.: Improved
657 confidence in climate change projections of precipitation evaluated using daily statistics from
658 the PRUDENCE ensemble, Clim. Dyn., 32**,** 1097-1106, 2009.

659 Byrne, M.P., Pendergrass, A.G., Rapp, A.D., and Wodzicki, K.R.: Response of the
660 Intertropical Convergence Zone to Climate Change: Location, Width, and Strength, Curr.
661 Clim. Chang. Reports, 4, 355-370, 2018.

662 Chen, D., and Dai, A.: Dependence of estimated precipitaiton frequency and intensity
663 on data resolution, Clim. Dyn., 50, 3625-3647, 2018.

664 Chen, C.T., and Knutson, T.: On the verification and comparison of extreme rainfall
665 indices from climate models, J. Climate, 21, 1605-1621, 2008.

666 Chou, C., Chen, C.-A., Tan P.-H., and Chen, K.T.: Mechanisms for global warming
667 impacts on precipitation frequency and intensity, J. Clim., 25, 3291-3306, 2012.

668 Christensen, J.H., and Christensen, O.B.: Climate modeling: Severe summertime
669 flooding in Europe, Nature, 421, 805-806, 2003.

670 Diffenbaugh, N.S, Giorgi, F., Raymond, L., and Bi, X.: Indicators of 21st century
671 socioclimatic exposure. Proc. Nat. Acad. Sci., 104, 20195-20198.

672 Easterling, D.R., Meehl, G.A., Parmesan. C., Changnon, S.A., and Mearns, L.O.:
673 Climate extremes: Observations, modeling and impacts, Science, 289, 2068-2074, 2000.

674 Fischer, E.M., and Knutti, R.: Observed heavy precipitation increase confirms theory
675 and early models, Nature Climate Change, 6, 986-990, 2016.

676 Flato, G., Marotzke, J., Abiodun, B., Bracconot, P., Chou, S.C., Collins, W., Cox, P.,
677 Driouech, F., Emori, S., Eyring, V., Forest, C., Glecker, P., Guiliard, E., Jacob, C., Kattsov,

678 V.,Reason, C., and Rummukainen, M.: Evaluation of climate models. Chapter 9 of Climate
679 Change 2013. The Physical Science Basis. Contribution of Working Group I to the Fifth
680 Assessment Report of the Intergovernmental Panel on Climate Change, Stocker T.F., et al.,
681 Eds., Cambridge University Press, Cambridge, United Kingdom and New York, NY, USA,
682 pp. 741-866, 2013.

683 Gao, X.J., Pal, J.S., and Giorgi, F.: Projected changes in mean and extreme
684 precipitation over the Mediterranean region from high resolution double nested RCM
685 simulations, Geophys. Res. Lett., 33, L03706, 2006.

686 Giorgi, F., and Bi, X.: Regional changes in surface climate interannual variability for
687 the 21st century from ensembles of global model simulations, Geophys. Res. Lett., 32,
688 L13701, 2005.

689 Giorgi, F., and Coppola, E.: Projections of 21st century climate over Europe, European
690 Physical Journal, Web of Conferences, 1, 29-46, 2009.

691 Giorgi, F., Shields Brodeur, C., and Bates G.T.: Regional climate change scenarios
692 over the United States produced with a nested regional climate model, J. Climate, 7, 375-399,
693 1994.

694 Giorgi, F., Jones, C., and Asrar, G.: Addressing climate information needs at the
695 regional level: The CORDEX framework, WMO Bulletin, 58, 175-183, 2009.

696 Giorgi, F., Im, E.-S., Coppola, E., Diffenbaugh, N.S., Gao, X.J., Mariotti, L., and Shi,
697 Y.: Higher hydroclimatic intensity with global warming, J. Climate, 24, 5309-5324, 2011.

698 Giorgi, F., Coppola, E., Solmon, F., Mariotti, L., Sylla, M.B., Bi, X., Elguindi, N.,
699 Diro, G.T., Nair, V., Giuliani, G., Turuncoglu, U.U., Cozzini, S., Guttler, I., O'Brien, T.A.,
700 Tawfik, A.B., Shalaby, A., Zakey, A.S., Steiner, A.L., Stordal, F., Sloan, L.C., and Brankovic,

C.: RegCM4: Model description and preliminary tests over multiple CORDEX domains, Clim. Res., 52, 7-29, 2012.

Giorgi, F., Coppola, E., Raffaele, F., Diro, G.T., Fuentes-Franco, R., Giuliani, G., Mamgain, A., Llopart-Pereira, M., Mariotti, L., and Torma, C.: Changes in extremes and hydroclimatic regimes in the CREMA ensemble projections, Climatic Change, 125, 39-51, 2014a.

Giorgi, F., Coppola, E., and Raffaele, F.: A consistent picture of the hydroclimatic response to global warming from multiple indices: Modeling and observations, J. Geophys. Res., 119, 11,695-11,708, 2014b.

Giorgi, F., Torma, C., Coppola, E., Ban, N., Schar, C., and Somot, S.: Enhanced summer convective rainfall at Alpine high elevations in response to climate warming, Nature Geoscience, 9, 584-589, 2016.

Giorgi, F., Coppola, E., and Raffaele, F.: Threatening levels of cumulative stress due to hydroclimatic extremes in the 21st century. NPJ Climate and Atmospheric Science, 1, 18, doi:10.1038/s41612-018-0028-6, 2018.

Gutowski, W.J. Jr., Takle, E.S., Kozak, K.A., Patton, J.C., Arritt, R.W., and Christensen, J.C.: A possible constraint on regional precipitation intensity changes under global warming, J. Hydrometeorol., 8, 1382-1396, 2007.

Gutowski, W.J. Jr, Giorgi, F., Timbal, B., Frigon, A., Jacob, D., Kang, H.-S., Krishnan, R., Lee, B., Lennard, C., Nikulin, G., O'Rourke, E., Rixen, M., Solman, S., Stephenson, T., and Tangang, F.: WCRP Coordinated Regional climate Downscaling Experiment (CORDEX): A diagnostic MIP for CMIP6 Geoscientific Model Development, 9, 4087-4095, 2016.

Intergovernmental Panel on Climate Change (IPCC). Managing the risks of extreme events and disasters to advance climate change adaptation, IPCC Special Report, Field C.B., et al., Eds., Cambridge University Press, Cambridge, U.K., 582 pp, 2012.

Intergovernmental Panel on Climate Change (IPCC). Climate Change 2013. The Physical Science Basis. Contribution of Working Group I to the Fifth Assessment Report of the Intergovernmental Panel on Climate Change, Stocker T.F., et al., Eds., Cambridge University Press, Cambridge, United Kingdom and New York, NY, USA, 1029 pp, 2013.

Held, I.M., and Soden, B.J.; Robust responses of the hydrological cycle to global warming, J. Climate, 19, 5686-5699, 2006.

Herold, N., Behrangi, A., and Alexander, L.V.: Large uncertainties in observed daily precipitation extremes over land, J. Geophys. Res. Atmos., 122**,** 668-681, 2017.

Ivancic, T.J., and Shaw, S.B.: A U.S. based analysis of the ability of the Clausius-Clapeyron relationship to exaplin changes in extreme rainfall with changing temperature, J. Geophys. Res. Atmos., 121, 3066-3078, 2016.

Jacob, D., Petersen, J., Eggert, P., Alias, A., Christensen, O.B., Bouwer, L.M., Braun, A., Colette, A., Deque, M., Georgievski, G., Georgopoulou, E., Gobiet, A., Menut, L., Nikulin, G., Haensler, A., Hampelmann, N., Jones, C., Keuler, K., Kovats, S., Kroner, N., Kotlarski, S., Kriegsmann, A., Martin, E., van Meijgaard, E., Moseley, C., Pfeifer, S., Preuschmann, S., Radermacher, C., Radtke, K., Rechid, D., Rounsevell, M., Samuelsson, P., Somot, S., Soussana, J.F., Teichmann, C., Valentini, R., Vautard, R., Weber, B., and Yiou, P.: EURO-CORDEX: New high resolution climate change projections for European impact research, Regional Environmental Change, 14**,** 563-578, 2014.

746 Jones, C., Giorgi, F., and Asrar, G.: The COordinated Regional Downscaling
747 EXperiment: CORDEX. An international downscaling link to CMIP5, CLIVAR Exchanges,
748 16, 34-40, 2011.

749 Kharin, V.V., Zwiers, F.W., and Zhang, X.: Intercomparison of near surface
750 temperature and precipitation extremes in AMIP-2 simulations, reanalyses and observations,
751 J. Climate, 18, 5201-5233, 2005.

752 Lenderink, G., and van Meijgaard, K.: Increase in hourly extreme precipitaiton beyond
753 expectations from temperature change, Nature Geoscience, 1, 511-514, 2008.

754 Moss, R.H., Edmonds, J.A., Hibbard, K.A., Manning, M.R., Rose, S.K., van Vuuren,
755 D.P., Carter, P.R., Emori, S., Kainuma, M., Kram, T., Meehl, G.A., Mitchell, J.F.B.,
756 Nakicenovic, N., Rihai, K., Smith, S.J., Stouffer, R.J., Thompson, A.M., Weyant, J.P., and
757 Willbanks, T.J.: The next generation of scenarios for climate change research and assessment,
758 Nature, 463, 747–756, 2010.

759 Mueller, C.J., and Held, I.M.: Detailed investigation of the self-aggregation of
760 convection in cloud-resolving simulations. J. Atm Sci., 69, 2551-2565, 2012.

761 Pall, P., Allen, M.R., and Stone, D.A.: Testing the Clausius-Clapeyron constraint on
762 changes in extreme precipitaiton under CO_2 warming, Clim. Dyn., 28, 351-363, 2007.

763 Pendergrass, A.G., and Hartmann, D.L.: Changes in the distribution of rain frequency
764 and intensity in response to global warming, J. Clim., 27, 8372-8383, 2014.

765 Pendergrass, A.G., Knutti, R., Lehner, F., deser, C., and Sanderson, B.M.:
766 Precipitation variability increases in a warmer climate, Sci. Rep., 7, 17966, 2017.

767 Pfahl, S., O'Gorman, P.A., and Fischer, E.M.: Understanding the regional pattern of
768 projected future changes in extreme precipitation. Nat. Clim. Chang., 7, 4230427, 2017.

769 Power, S., Delage, F., Chung, C., Kociuba, G., and Keay, K.: Robust twenty-first
770 century projections of El-Nino and related precipitation variability, Nature, 502, 541-545,
771 2013.

772 Prein. A.F., Langhans, W., Fosser, G., Ferrone, A., Ban, N., Goergen, K., Keller, M.,
773 Tolle, M., Gutjahr, O., Feser, F., Brisson, E., Koller, S., Schmidli, J., van Lipzig, N.P.M.,
774 Leung, R.: A review on regional convection-permitting climate modeling: Demonstrations,
775 prospects and challenges, Rev. Geophys., 53, 323-361, 2015.

776 Raisanen, J.: CO_2 - induced changes in interannual temperature and precipitation
777 variability in 19 CMIP2 experiments, J. Climate, 15, 2395-2411, 2002.

778 Rihai, K., van Vuuren, D.P., Kriegler, E., Edmonds, J., O'Neill, B.C., Fujimori, S.,
779 Bauer, N., Calvin, K., Dellink, R., Fricko, O., Luta, W., Popp, A., Cuaresma, J.C., Samir,
780 K.C., Leimbach, M., Jiang, L., Kram, T., and Rao, S.: The Shared Socioeconomic Pathways
781 and their energy, land use, and greenhouse gas emissions implications: An Overview, Global
782 Environmental Change, 42, 153-168, 2016.

783 Ruti, P., Somot, S., Giorgi, F., Dubois, C., Flaounas, E., Obermann, A., Dell'Aquila,
784 A., Pisacane, A., Harzallah, A., Lombardi, E., Ahrens, B., Akhtar, N., Alias, A., Arsouze, T.,
785 Aznar, R., Bastin, S., Bartholy, J., Beranger, K., Beuvier, J., Bouffies-Cloche, S., Brauch, J.,
786 Cabos, W., Calmanti, S., Calvet, J.C., Carillo, A., Conte, D., Coppola, E., Djurdjevic, V.,
787 Drobinski, P., Elizalde, A., Gaertner, M., Galan, P., Gallardo, C., Goncalves, M., Gualdi, S.,
788 Jorba., O., Jorda, G., Lheveder, B., Lebeaupin-Brossier, C., Li, L., Liguori, G., Lionello, P.,
789 Macias-Moy, D., Nabat, P., Onol, B., Rajkovic, B., Ramage, K., Sevault, F., Sannino, G.,

790 Struglia, M.V., Sanna, A., Torma, G., and Vervatis, V.: MED-CORDEX initiative for
791 Mediterranean climate studies, Bull. Am. Met. Soc., 97, 1187-1208, 2016.

792 Schiemann, R., Demory, M.-E., Shaffrey, L.C., Strachan, J., Vidale, P.L., Mizielinski,
793 M.S., Roberts, M.J., Matsueda, M., Wehner, M.F., and Jung, T.: The resolution sensitivity of
794 northern hemisphere blocking in 4 25-km atmospheric global circulation models, J. Climate,
795 30, 337-358, 2017.

796 Sedalcek, J., and Knutti, R.: Half of the World's population experience robust changes
797 in the water cycle for a 2C warmer World, Environ. Res. Lett., 9, 044008, 2014.

798 Sillmann, J., Kharin, V.V., Zwiers, F.V., Zhang, X., and Bronaugh, D.: Climate
799 extreme indices in the CMIP5 multimodel ensemble: Part 2. Future climate projections, J.
800 Geophys. Res., 118, 2473-2493, 2013a.

801 Sillmann, J., Kharin, V.V., Zhang, X., Zwiers, F.W., and Bronaugh, D.: Climate
802 extreme indices in the CMIP5 multimodel ensemble. Part I: Model evaluation in the present
803 climate, J. Geophys. Res., 118, 1716-1733, 2013b.

804 Taylor, K.E., Stouffer, R.J., and Meehl, G.A.: An Overview of CMIP5 and the
805 Experiment Design, Bull. Amer. Meteor. Soc., 93, 485–498, 2012.

806 Tebaldi, C., Hayhoe, K., Arblaster, J.M., and Meehl, G.A.: Going to the extremes: An
807 intercomparison of model-simulated historical and future changes in extreme events, Climatic
808 Change, 79, 185-211, 2006.

809 Thackeray, C.W., DeAngelis, A.M., Hall, A., Swain, D.L., and Qu, X.: On the
810 connection between global hydrologic sensitivity and regional wet extremes, Geophys. res.
811 Lett., doi:10.1029/2018GL079698, 2018.

812 Trenberth, K.E.: Conceptual framework for changes of extremes of the hydrological
813 cycle with climate change, Clim. Change, 42, 327-339, 1999.

814 Trenberth, K.E.: Changes in precipitation with climate change, Clim. Res. 47, 123-
815 138, 2011.

816 Trenberth, K.E., Dai, A., Rasmussen, R.M., and Parsons, D.B.: The changing
817 character of precipitation, Bull. Am. Meteor. Soc., 84, 1205-1217, 2003.

818 Trenberth, K.E., Smith, L., Qian, T., Dai, A., and Fasullo, J.: Estimates of the global
819 water budegt and its annual cycle using observational and model data, J. Hydrometeorology,
820 8, 758-769, 2007.

821 Warner, T.T.: Numerical Weather and Climate Prediction, Cambridge University
822 Press, Cambridge U.K., 526 pp., 2010.

823 Wehner, M.F., Smith, R.L., Bala, G., and Duffy, P.: The effect of horizontal resolution
824 on simulaiton of very extreme US precipitation events in a global atmosphere model, Clim.
825 Dyn., 24**,** 241-247, 2010.